

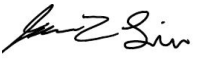
SCHOOL OF MECHATRONIC SYSTEMS ENGINEERING
SIMON FRASER UNIVERSITY

MSE 211: Computational Methods for Engineers

Final Project: Design of a Four-Bar Mechanism for Gardening

April 3, 2019

Group number: 13

James Zhong Sheng Liu 301310205 

Junaid Jawed Khan 301308300 

Syed Salman Haider Abdi 301308300 

Eric Alfred Herbert 301333452 

Abstract

In this project, a four-bar mechanism designed for gardening was created and analyzed. The overall goal was an easy-to-operate garden tool with smooth motion and simple operation. The mechanism was created using the function generation algorithm to determine link lengths and relative link angles as well as bisection method to create an animation of the motion in MATLAB. Initial angles were estimated and function generation was used to fit these parameters to the desired precision points. It was calculated that having the input and output links the same length resulted in the best path of motion. The prototype was constructed from a thin sheet of MDF. The prototype executed smooth motion just as desired. Considering the lightweight properties of MDF with the given dimensions, recommended choice of materials for future full-scale prototypes would be lightweight metals such as aluminum or a wood such as oak or ash.

Introduction	3
Figure 1: Generic Four-Bar Mechanism	3
Figure 2: Hoe, Rake, Spade (left to right)	3
Description of the Task	4
Figure 3: Four Precision Points from Initial Planning	4
Figure 4: Six equations utilized for the Function Generation Algorithm (for j=1:1:3)	4
Figure 5: Plot of the final design's precision points	4
Figure 6: Pictures of the 4 mechanical-cycle frames	5
Design of the Mechanism	5
Figure 7: Initial values and guesses for Function Generation (Fval = 0.00037485)	5
Figure 8: Improved initial values and guesses for Function Generation (Fval = 0.00013534)	5
Figure 9: Lengths of frame, input, coupler, and follower links respectively with Fval	6
Figure 10: Plot of the initial and improved configurations	6
Figure 11: Mechanism with Beta and Gamma angles	7
Figure 12: Function generation equations with variables in place for estimated starting points	7
Kinematic Analysis	8
Figure 13: Angular displacement of Input θ_2 vs Coupler θ_3	8
Figure 14: Angular displacement of Input θ_2 vs Output θ_3	8
Figure 15: Equations used to solve for θ_2 , θ_3 , and θ_4	9
Figure 16: Plots for θ_2 vs center of mass displacement	9
Figure 17: Equations used to find angular velocity	9
Figure 18: Plots for θ_2 vs angular velocity for θ_3 and θ_4	10
Figure 19: Plots for θ_2 vs angular acceleration for θ_3 and θ_4	10
Figure 20: Plots for θ_2 vs linear velocity of input link's CoM (x, y)	10
Figure 21: Plots for θ_2 vs linear velocity of coupler link's CoM (x, y)	11
Figure 22: Plots for θ_2 vs linear velocity of output link's CoM (x, y)	11
Figure 23: Plots for θ_2 vs linear acceleration of input link's CoM (x, y)	11
Figure 24: Plots for θ_2 vs linear acceleration of coupler link's CoM (x, y)	12
Figure 25: Plots for θ_2 vs linear acceleration of output link's CoM (x, y)	12
Dynamic Analysis	13
Figure 26: Solidworks analysis of each link	13
Figure 27: Mass and inertia properties of each link	15
Figure 28: Reaction forces and torque solved in Matlab	16
Figure 29: System of equations in Matlab	16
Figure 30: Graph of input torque vs θ_2	17
Coupler Curve Analysis	17
Figure 31: Graph of coupler vs θ_2 (x direction)	18
Figure 32: Graph of coupler vs θ_2 (y direction)	18
Conclusion	19
References	20

Introduction

A four-bar mechanism (linkage) is a mechanical system which consists of four bodies connected at four pivot points. The four bodies are called the frame, input, coupler, and follower (also referred to as output link). The frame is a fixed body that will be used as the reference-frame for any movement generated by the input link. The input link takes the input motion and transfers it to the follower, directed by the coupler link. The three moving links work in conjunction to generate the desired motion at the end-effector. In this case, the four-bar mechanism will be employed as a gardening tool.

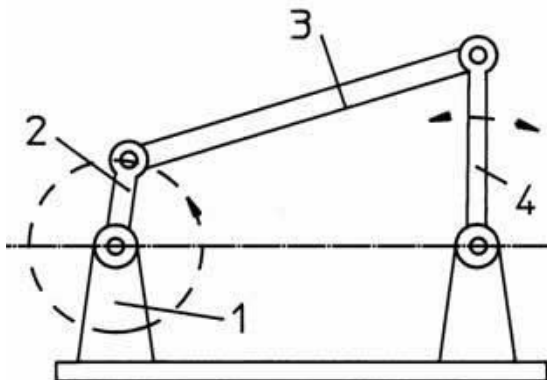


Figure 1: Generic Four-Bar Mechanism

The gardening tool was designed to create a ‘clawing’ motion meaning that the end effector would have to move in both the x and y-axis, from a planar perspective. The whole idea is that the end-effector should be modifiable such that any tool could be attached to the end; similar to the function of a hand-drill. A selection of shovels, rakes, and hoes could be attached to the output node of our four-bar mechanism such that the user would be able to accomplish a variety of tasks with the same mechanism.



Figure 2: Hoe, Rake, Spade (left to right)

This idea was birthed when the issue of elderly-gardeners came to mind. It seems that gardening is a leisurely activity that the elderly tend to pick up. Hours spent hunched over a garden could be strenuous to one’s back and discourage one from spending a length of time tending to a garden. This tool is designed to help the user complete a repeatable task over and over without tiring out. Although this application is better suited towards those who tend to large gardens, it is a handy tool that could greatly benefit anyone with an aching to grow vegetation.

Description of the Task

The initial step was generating a design with a focus on the four critical precision points of the desired motion. After determining the four precision points, the points could then be used as estimates for our function generation algorithm. Figure 3 shows the four precision points from the initial design planning phase.

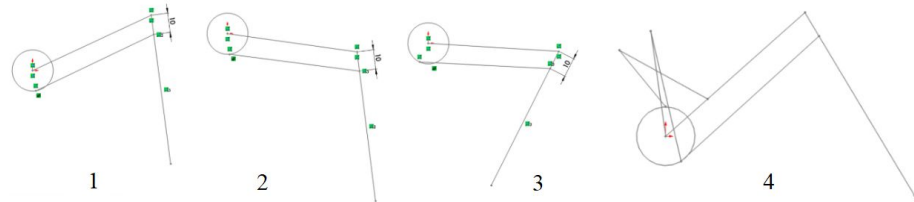


Figure 3: Four Precision Points from Initial Planning

However, it was decided that the initial design was a bit more complex than what was desired. Thus, we revised our initial design and came up with a more suitable design. The first precision point is the starting position, the second precision point raises the end-effector up, the third precision point lowers the end-effector down, and the fourth precision point slightly pulls the end-effector towards the input node, consequently completing a full cycle.

$$f_{jx} = -r_{2x} \cos(\beta_j) + r_{2y} \sin(\beta_j) - r_{3x} \cos(\varphi_j) + r_{3y} \sin(\varphi_j) + r_{4x} \cos(y_j) - r_{4y} \sin(y_j) + r_{2x} + r_{3x} - r_{4x} = 0$$

$$f_{jy} = -r_{2x} \sin(\beta_j) - r_{2y} \cos(\beta_j) - r_{3x} \sin(\varphi_j) - r_{3y} \cos(\varphi_j) + r_{4x} \sin(y_j) + r_{4y} \cos(y_j) + r_{2y} + r_{3y} - r_{4y} = 0$$

$$F = \sqrt{(f_{1x})^2 + (f_{1y})^2 + (f_{2x})^2 + (f_{2y})^2 + (f_{3x})^2 + (f_{3y})^2}$$

Figure 4: Six equations utilized for the Function Generation Algorithm (for $j=1:1:3$)

The six equations detailed in figure 4 consist of 3 sets of two equations; one set each for x and y. The initial point (starting position) is a given value that we set; thereby only requiring the solutions of 3 sets of two equations, instead of 4 sets of two equations. The function generation algorithm solves for the distances and displacements of each consequent point that comes after the initial point.

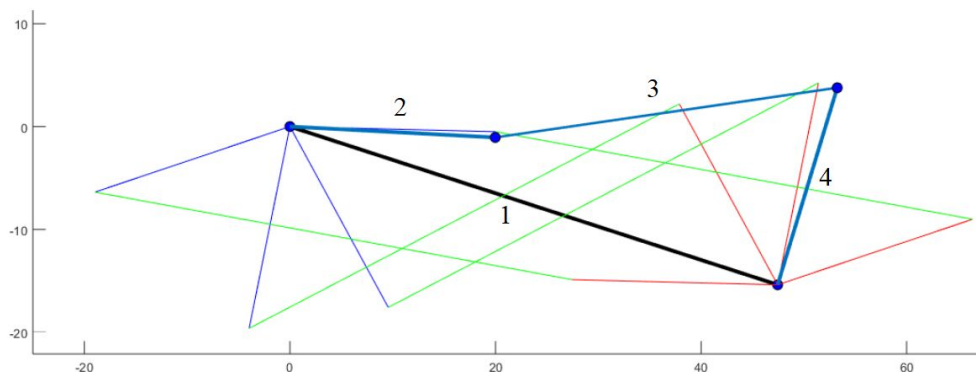


Figure 5: Plot of the final design's precision points

In figure 5, the 4 links are illustrated by the one black line and the three blue lines labelled 1 (frame), 2 (input), 3 (coupler), and 4 (follower). The coordinates of $(R_{2x}, R_{2y}) = (20, -0.5)$ reveal the first point; where the input link starts. The input link starts at around a 30° angle, relative to the frame link. The input link rotates in the clockwise direction for about 130° . The input link then reverses in the counterclockwise direction for the same amount; this is equivalent to one cycle for our four-bar mechanism. Figure 6 depicts the 4 frames that our four-bar mechanism goes through to complete one mechanical-cycle. It is also a good reflection of how accurately the physical model corresponds to the calculated frames in figure 5.

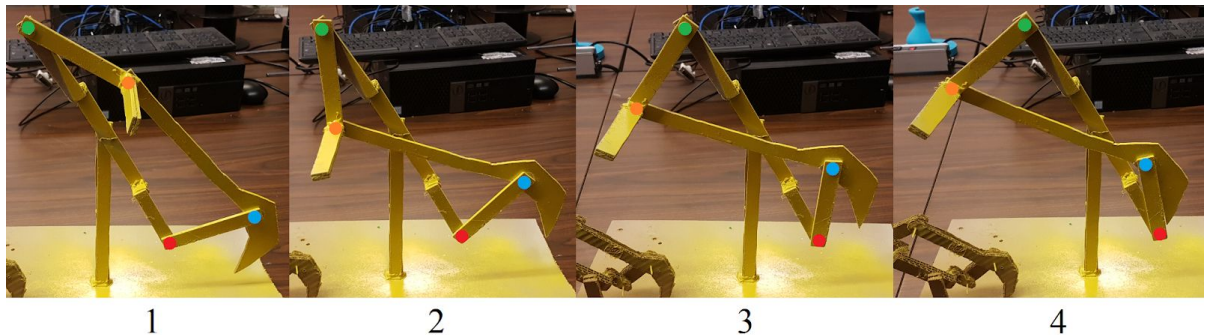


Figure 6: Pictures of the 4 mechanical-cycle frames

Design of the Mechanism

The equations shown in figure 4 were used to determine the level of suitability of the chosen initial values and guesses. When it comes to the evaluation of the objective function, it is most desirable to have a value as close to 0. The previous iteration leads to a function evaluation value of 0.00037485. The current iteration function evaluation number sits at 0.00013534. The former value was acceptable but it was made better by changing the input variables fundamental to the objective function.

R_{2x}	R_{2y}	R_{3x}	R_{3y}	R_{4x}	R_{4y}	β_1	β_2	β_3	ϕ_1	ϕ_2	ϕ_3	γ_1	γ_2	γ_3
20	-0.5	45	-2	20	2	$\frac{-\pi}{4}$	$\frac{-\pi}{2}$	$\frac{-13\pi}{18}$	$\frac{\pi}{6}$	$\frac{3\pi}{4}$	$\frac{8\pi}{9}$	$\frac{\pi}{4}$	$\frac{\pi}{2}$	$\frac{13\pi}{18}$

Figure 7: Initial values and guesses for Function Generation ($Fval = 0.00037485$)

R_{2x}	R_{2y}	R_{3x}	R_{3y}	R_{4x}	R_{4y}	β_1	β_2	β_3	ϕ_1	ϕ_2	ϕ_3	γ_1	γ_2	γ_3
20	-0.5	45	-2	20	2	$\frac{-\pi}{3}$	$\frac{-5\pi}{9}$	$\frac{-8\pi}{9}$	$\frac{\pi}{6}$	$\frac{3\pi}{4}$	$\frac{8\pi}{9}$	$\frac{\pi}{3}$	$\frac{5\pi}{9}$	$\frac{8\pi}{9}$

Figure 8: Improved initial values and guesses for Function Generation ($Fval = 0.00013534$)

The critical changes made to the initial values were the beta (β) and gamma (γ) values. These are the angles between the frame & input as well as frame & follower links. The x and y coordinates of the precision points were left untouched because those are the constants that determine the points that the mechanism has to pass through. The changes in the initial guesses set up a different configuration for the four-bar mechanism and thus alters the motion of our mechanism.

The beta values signify the rotation (in radians) of the input link through each precision point relative to the first precision point. Similarly, the gamma values signify the rotation (in radians) of the output link through the precision points relative to the first precision point. Therefore, changing the beta and gamma values result in the algorithm returning different lengths for the links. Accordingly, the beta and gamma values had to be iterated upon so that the generated motion would be similar to what was desired. Figure 9 shows the difference in the dimensions of the links based on the initial values and guesses of the second-last and last iteration. The notable changes are the lengths of r_1 (frame), r_3 (coupler), and r_4 (follower). Figure 10 illustrates the two mechanism configurations; initial configuration on the left and improved configuration on the right.

Initial Values and Guesses				
Fval	r1	r2	r3	r4
0.00031558	54.49281690	20.00624902	48.48543091	19.82327487

Improved Initial Values and Guesses				
Fval	r1	r2	r3	r4
0.00013534	49.87959730	20.00624902	47.18826297	20.00631386

Figure 9: Lengths of frame, input, coupler, and follower links respectively with Fval

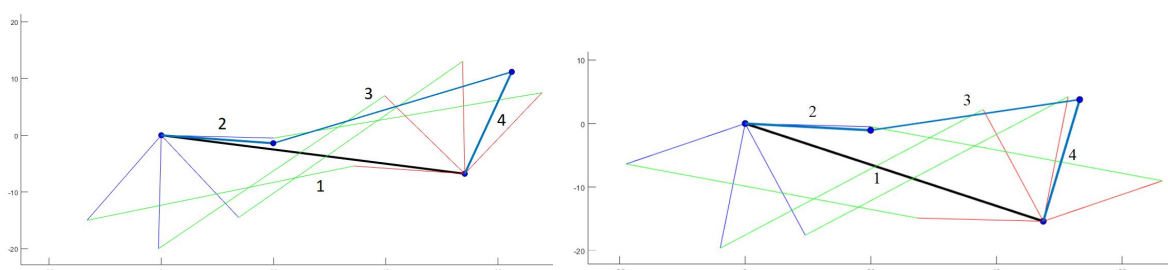


Figure 10: Plot of the initial and improved configurations

It took multiple random guesses to start the design process. After the random guesses generated a mechanism that more resembled the desired mechanism, a few approximated iterations closed the gap and led to the final design that you see on figure 5 and on the right side of figure 10. Figure 9 shows the final two iterations of the initial values and guesses along with their respective evaluated objective function values. The function generation equations have their effects on the objective function altered when the beta (β) and gamma (γ) values change.

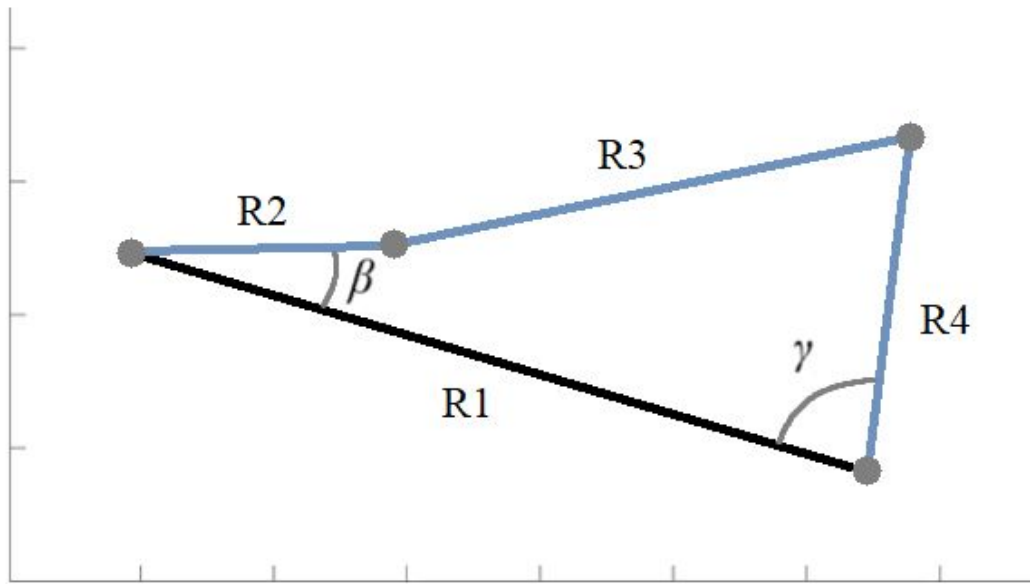


Figure 11: Mechanism with Beta and Gamma angles

Figure 11 specifies where the beta and gamma angles are located on our mechanism along with the respective R_j vector labels for each link. The first two equations (repeated three times for $j=1:1:3$) in figure 12 are solved as a matrix with the use of the R_j vectors and the beta, phi, and gamma angles. The [x,y] vectors for R_3 and R_4 as well as the values for $\varphi_{1,2,3}$ (phi) are unknowns that are equated to variables ‘a’ through ‘g’. Then using the MatLab function, *fminunc*, the objective function is minimized till the point $F = 0$. *fminunc* accomplishes this through the method of finding a minimum value for an unconstrained multivariable function (i.e. the objective function used here).

$$f_{jx} = -r_{2x} \cos(\beta_j) + r_{2y} \sin(\beta_j) - r_{3x} \cos(\varphi_j) + r_{3y} \sin(\varphi_j) + r_{4x} \cos(\gamma_j) - r_{4y} \sin(\gamma_j) + r_{2x} + r_{3x} - r_{4x} = 0$$

$$f_{jy} = -r_{2x} \sin(\beta_j) - r_{2y} \cos(\beta_j) - r_{3x} \sin(\varphi_j) - r_{3y} \cos(\varphi_j) + r_{4x} \sin(\gamma_j) + r_{4y} \cos(\gamma_j) + r_{2y} + r_{3y} - r_{4y} = 0$$

Estimate starting points for the seven unknowns, i.e.,

$$r_{3x} = a \quad r_{3y} = b \quad r_{4x} = c \quad r_{4y} = d \quad \varphi_1 = e \quad \varphi_2 = f \quad \varphi_3 = g$$

Figure 12: Function generation equations with variables in place for estimated starting points

Kinematic Analysis

The displacement of the input link is characterized by θ_2 , coupler link by θ_3 , and the output link by θ_4 . The relationship between θ_2 and θ_3 is not linear. This means that finding the value of θ_3 based on the known value of θ_2 requires more complex calculations. As you can see in figure 13, the relationship between θ_2 and θ_3 exhibits the behavior of a quadratic. The reason this occurs is that the rate of change for θ_3 is higher than that of θ_2 . On the other hand, the relationship between θ_2 and θ_4 seems to exhibit the behaviour of a linear relationship, illustrated in figure 14. This is because the rate of change of θ_2 and θ_4 are almost equivalent due to the design of our four-bar mechanism. If you take into consideration the lengths of the links and the location of the θ angle you are observing, it makes more sense as to why one θ value might change quicker than the other. Ultimately, it is the fact that the input and output link in this four-bar mechanism share the same length, while the coupler link is much longer, that causes this relationship to hold between θ_2 and θ_3 as well θ_2 and θ_4 .

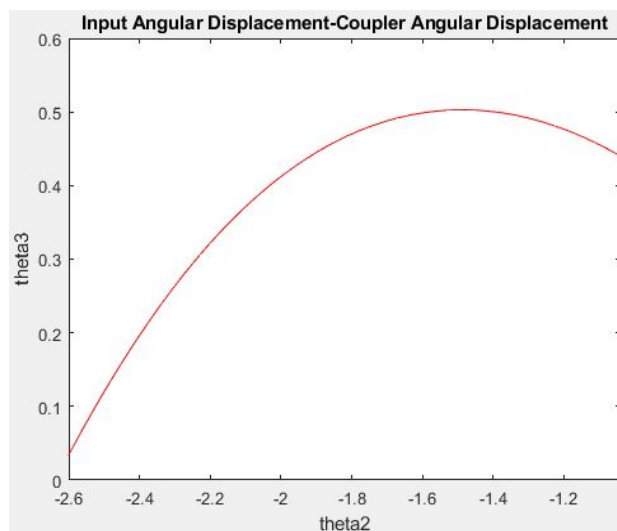


Figure 13: Angular displacement of Input θ_2 vs Coupler θ_3

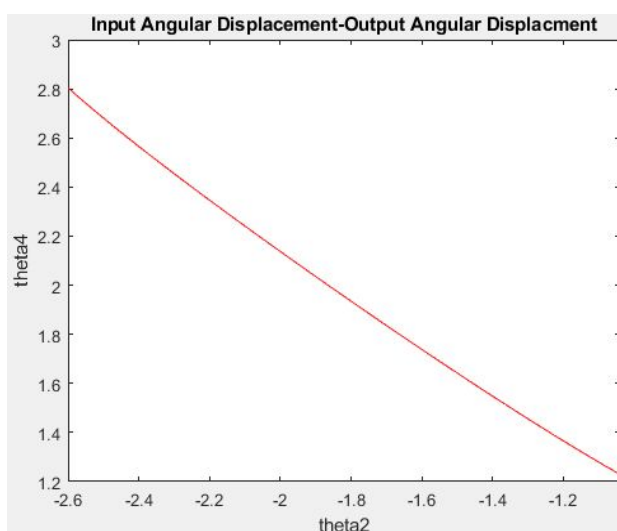


Figure 14: Angular displacement of Input θ_2 vs Output θ_3

The (1) equations in figure 15 are representative of the mechanism using vectors $\bar{R}_1, \bar{R}_2, \bar{R}_3$, and \bar{R}_4 and angles θ_2, θ_3 , and θ_4 . The (2) equations in figure 15 are the first step to solving for the values of the thetas. By running a root-finding Bisection method algorithm on the function $f(\theta_4)$, we can find values roots for θ_4 that work with θ_3 and θ_4 to minimize the objective function of the function generation algorithm.

$$\begin{aligned} -\bar{R}_1 + \bar{R}_2 + \bar{R}_3 - \bar{R}_4 &= \bar{0} \\ &\quad \left. \begin{array}{l} -r_1 + r_2 \cos \theta_2 + r_3 \cos \theta_3 - r_4 \cos \theta_4 = 0 \\ r_2 \sin \theta_2 + r_3 \sin \theta_3 - r_4 \sin \theta_4 = 0 \end{array} \right\} \quad (1) \end{aligned}$$

$$f(\theta_4) = a \cos(\theta_4) + b \sin(\theta_4) - c \quad \text{where } c = \frac{r_3^2 - a^2 - b^2 - r_4^2}{2r_4} \quad (2)$$

$$r_3 \cos \theta_3 = a + r_4 \cos \theta_4 \quad | \quad r_3 \sin \theta_3 = b + r_4 \sin \theta_4$$

Figure 15: Equations used to solve for θ_2 , θ_3 , and θ_4

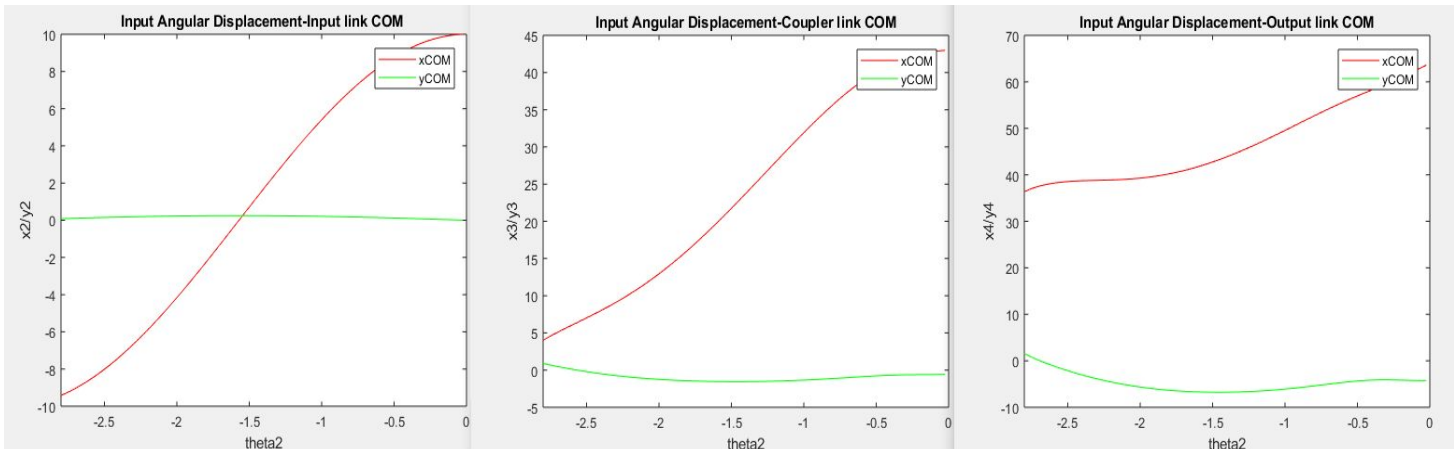


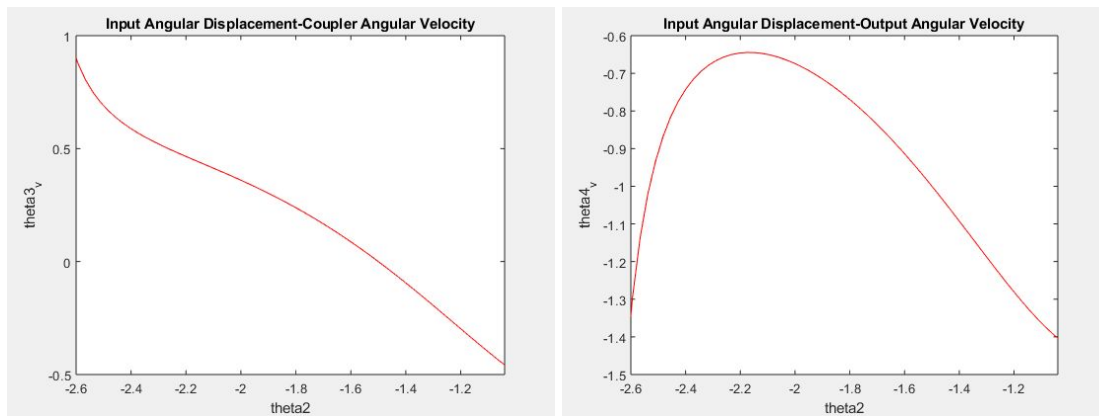
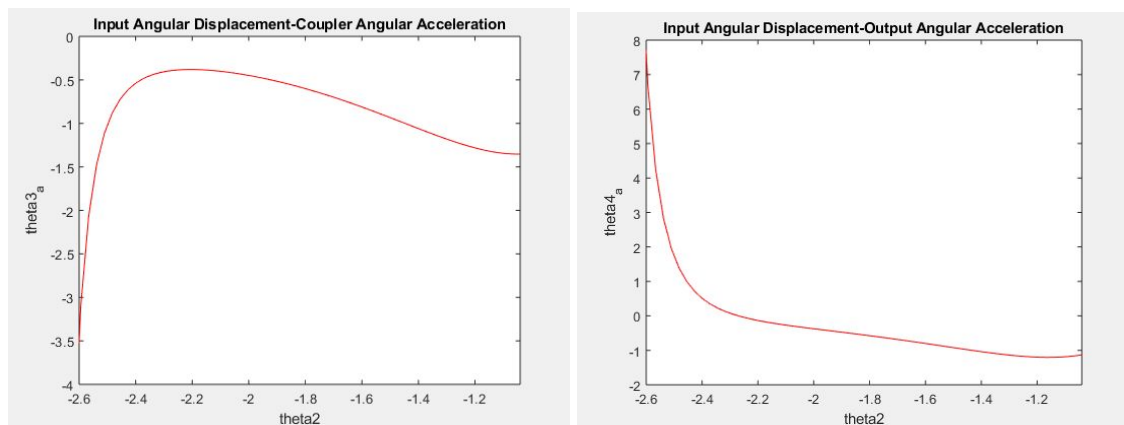
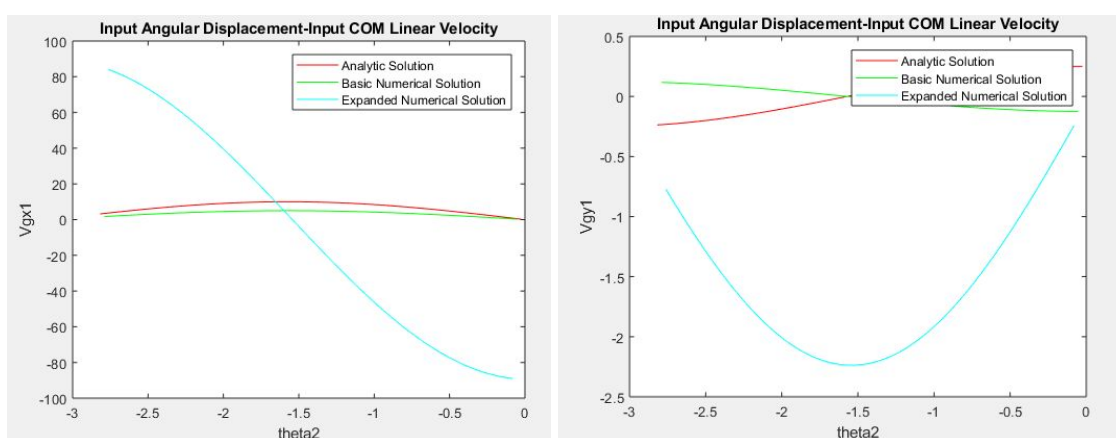
Figure 16: Plots for θ_2 vs center of mass displacement

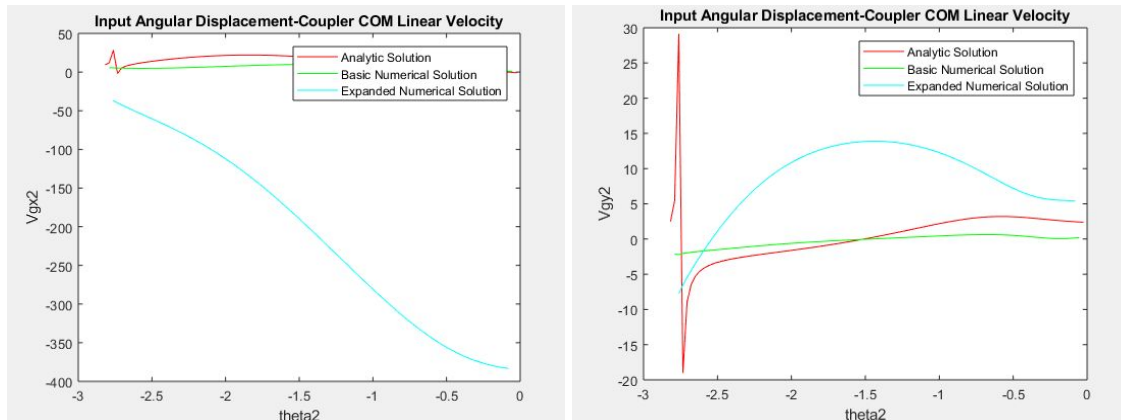
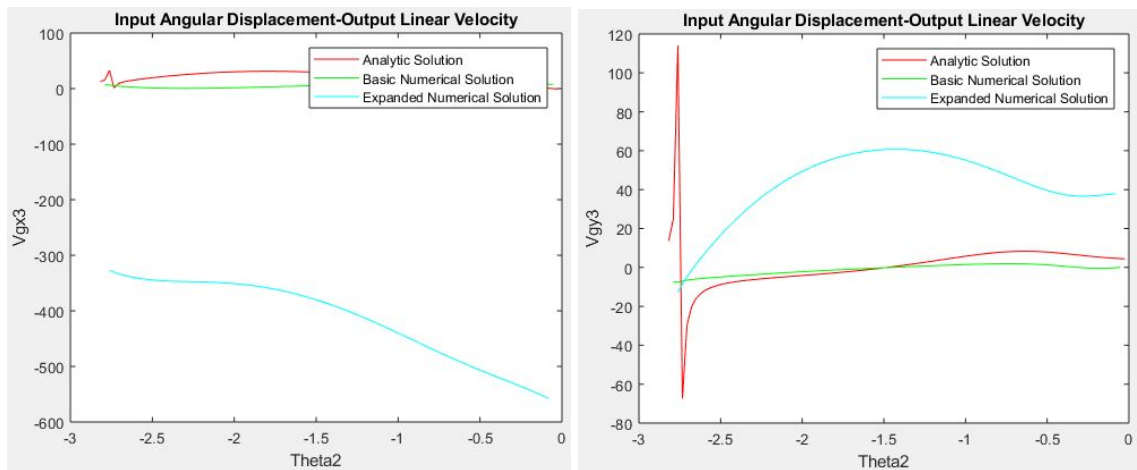
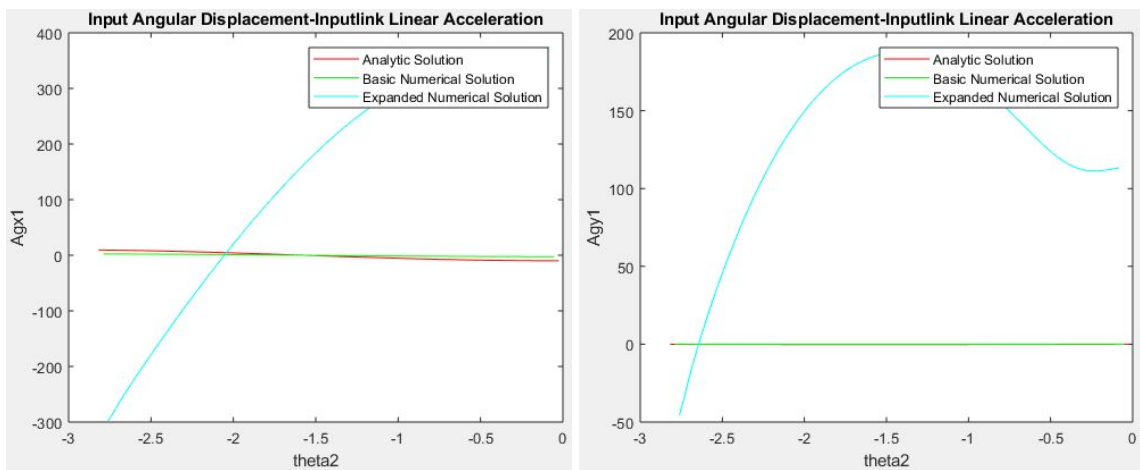
The plots in figure 16 show the displacement of the center of mass for the input (x_2, y_2), coupler(x_3, y_3), and output links (x_4, y_4) in relation to the change in θ_2 . The center of mass appears to change more in the x axis, according to the plots. This is reasonable because the links move more in the x direction than they do in the y direction.

Figure 18 shows the two plots for θ_2 compared to the angular velocities for θ_3 (left) and θ_4 (right). Figure 19 shows the two plots for θ_2 compared to the angular accelerations for θ_3 (left) and θ_4 (right). The data illustrated in the collective four plots were derived using the analytic method along with equations in figure 17.

$$\begin{aligned} -r_2 \sin \theta_2 \dot{\theta}_2 - r_3 \sin \theta_3 \dot{\theta}_3 + r_4 \sin \theta_4 \dot{\theta}_4 &= 0 \\ r_2 \cos \theta_2 \dot{\theta}_2 + r_3 \cos \theta_3 \dot{\theta}_3 - r_4 \cos \theta_4 \dot{\theta}_4 &= 0 \end{aligned} \quad \begin{array}{l} \text{Let input velocity be } \dot{\theta}_2, \text{ solve} \\ \text{for } \dot{\theta}_3 \text{ and } \dot{\theta}_4. \end{array}$$

Figure 17: Equations used to find angular velocity

Figure 18: Plots for θ_2 vs angular velocity for θ_3 and θ_4 Figure 19: Plots for θ_2 vs angular acceleration for θ_3 and θ_4 Figure 20: Plots for θ_2 vs linear velocity of input link's CoM (x, y)

Figure 21: Plots for θ_2 vs linear velocity of coupler link's CoM (x, y)Figure 22: Plots for θ_2 vs linear velocity of output link's CoM (x, y)Figure 23: Plots for θ_2 vs linear acceleration of input link's CoM (x, y)

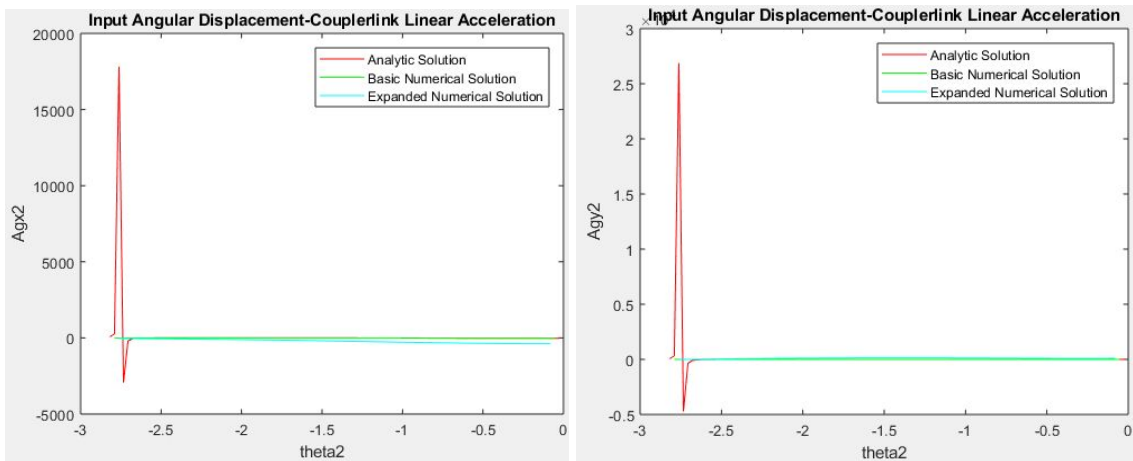


Figure 24: Plots for θ_2 vs linear acceleration of coupler link's CoM (x, y)

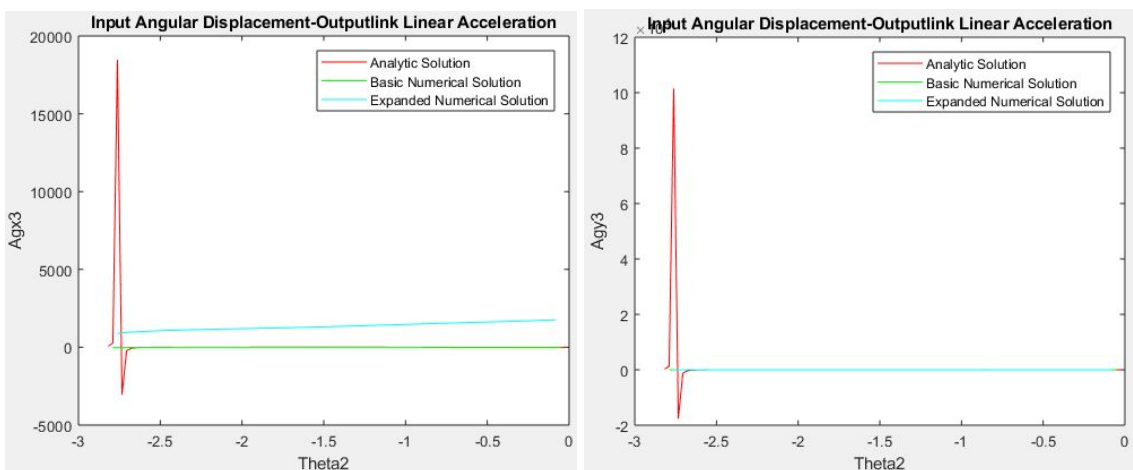


Figure 25: Plots for θ_2 vs linear acceleration of output link's CoM (x, y)

The plots in figure 20 through figure 22 present the data for θ_2 against linear velocity for the center of masses of the input, coupler, and output links in the x and y axes. The plots in figure 23 through figure 25 present the data for θ_2 against linear acceleration for the center of masses of the input, coupler, and output links in the x and y axes. The three lines in each of the plots are color coded to represent the three solutions found: red for analytic, green for basic numerical, and blue for expanded numerical. For the most part, the analytic solution and the basic numerical solution either are very similar or overlap fully. It is acceptable to say that they both produce approximately the same solution to the values for linear velocity and acceleration.

However, in the plots in figure 20 through figure 23, the expanded numerical solution plot lines are very distinct from the analytic and basic numerical solution plot lines. This dissimilarity stems from an error in the code which could not be fixed. Furthermore, the analytic solution plot lines have a spike in the plots on figure 21, 22, 24, and 25. It is hypothesized that these spikes signify the existence of a singularity point. This singularity point in our four-bar mechanism suggests that at a certain orientation our mechanism behaviour will be unpredictable to the extent that the velocity and acceleration can drastically change in a short period of time.

Dynamic Analysis

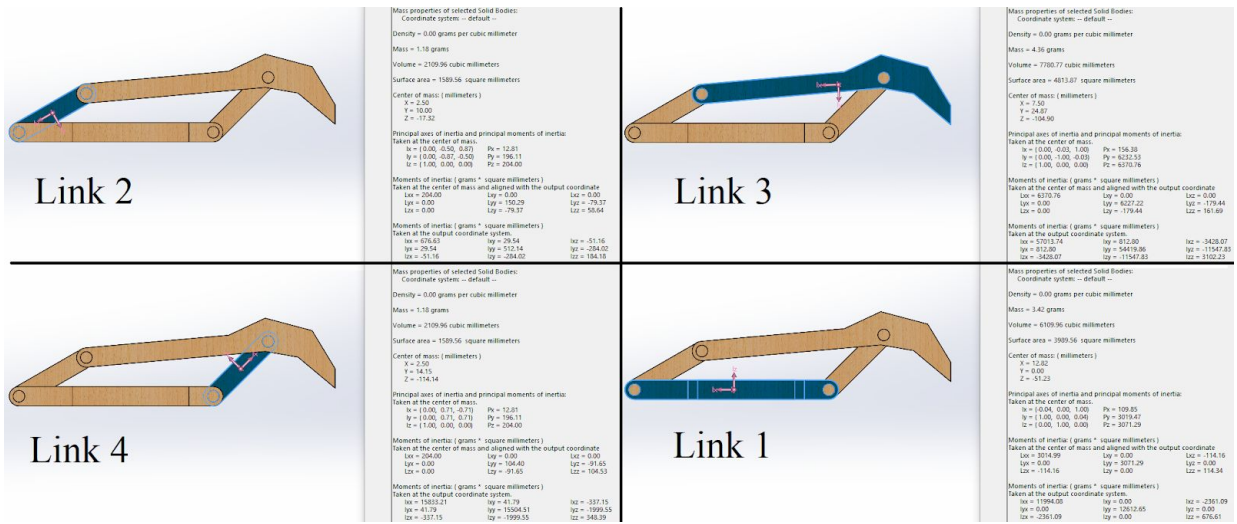
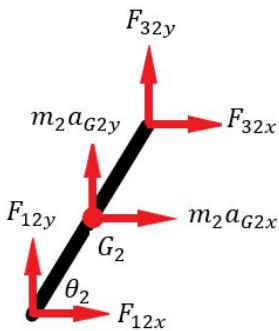


Figure 26: Solidworks analysis of each link

Analysis of Link 2

Link 2



$$\Sigma F_{2x} = m_2 a_{G2x} \quad (1)$$

$$\Sigma F_{2y} = m_2 a_{G2y} \quad (2)$$

$$\Sigma M_{G2} = I_{G2} + \theta_2'' \quad (3)$$

$$F_{12x} + F_{32x} = m_2 a_{G2x} \quad (1)$$

$$F_{12y} + F_{32y} = m_2 a_{G2y} \quad (2)$$

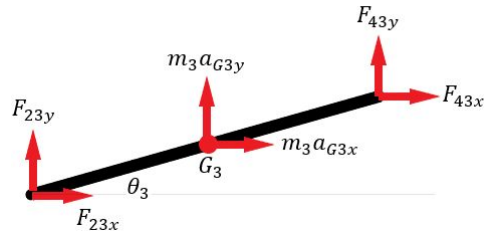
$$M_{12} + \frac{1}{2} r_2 \sin \theta_2 F_{12x} - \frac{1}{2} r_2 \cos \theta_2 F_{12y} - \frac{1}{2} r_2 \sin \theta_2 F_{32x} + \frac{1}{2} r_2 \cos \theta_2 F_{32y} = I_{G2} + \theta_2'' \quad (3)$$

This line will be re-written as:

$$M_{12} + a \cdot F_{12x} - b \cdot F_{12y} - a \cdot F_{32x} + b \cdot F_{32y} = I_{G2} + \theta_2'' \quad (3)$$

Analysis of Link 3

Link 3



$$\sum F_{3x} = m_3 a_{G3x} \quad (4)$$

$$\sum F_{3y} = m_3 a_{G3y} \quad (5)$$

$$\sum M_{G3} = I_{G3} + \theta_3'' \quad (6)$$

$$F_{23x} + F_{43x} = m_3 a_{G3x} \quad (4)$$

$$F_{23y} + F_{43y} = m_3 a_{G3y} \quad (5)$$

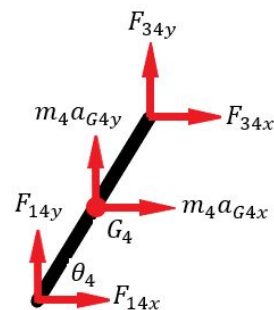
$$\frac{1}{2}r_3 \sin \theta_3 F_{23x} - \frac{1}{2}r_3 \cos \theta_3 F_{23y} - \frac{1}{2}r_3 \sin \theta_3 F_{43x} + \frac{1}{2}r_3 \cos \theta_3 F_{43y} = I_{G3} + \theta_3'' \quad (6)$$

This line will be re-written as:

$$c \cdot F_{23x} - d \cdot F_{23y} - c \cdot F_{43x} + d \cdot F_{43y} = I_{G3} + \theta_3'' \quad (6)$$

Analysis of Link 4

Link 4



$$\sum F_{4x} = m_4 a_{G4x} \quad (7)$$

$$\sum F_{4y} = m_4 a_{G4y} \quad (8)$$

$$\sum M_{G4} = I_{G4} + \theta_4'' \quad (9)$$

$$F_{14x} + F_{34x} = m_4 a_{G4x} \quad (7)$$

$$F_{14y} + F_{34y} = m_4 a_{G4y} \quad (8)$$

$$\frac{1}{2}r_4 \sin \theta_4 F_{14x} - \frac{1}{2}r_4 \cos \theta_4 F_{14y} - \frac{1}{2}r_4 \sin \theta_4 F_{34x} + \frac{1}{2}r_4 \cos \theta_4 F_{34y} = I_{G4} + \theta_4'' \quad (9)$$

This line will be re-written as:

$$e \cdot F_{14x} - f \cdot F_{14y} - e \cdot F_{34x} + f \cdot F_{34y} = I_{G4} + \theta_4'' \quad (9)$$

Newton's Third Law

$$F_{23x} + F_{32x} = 0 \quad (10)$$

$$F_{23y} + F_{32y} = 0 \quad (11)$$

$$F_{34x} + F_{43x} = 0 \quad (12)$$

$$F_{34y} + F_{43y} = 0 \quad (13)$$

Knowns

Link	Length, r (mm)	Mass, m (grams)	Moment of Inertia, I_{Gx} (gmm^2)	Moment of Inertia, I_{Gy} (gmm^2)
1	49.88	3.42	109.85	3019.47
2	20.01	1.18	12.81	196.11
3	47.19	4.36	156.38	6232.53
4	20.01	1.18	12.81	196.11

Figure 27: Mass and inertia properties of each link

$$\tau = M_{12}$$

Note: All masses and moments of inertia were found using solidworks.

The prototype was made from a single $\frac{1}{8}$ inch sheet of MDF. The calculated masses and inertia properties do correspond to the simple geometry of each link and the density of the material used. MDF is a light weight material when cut into pieces of this size, so the small mass and inertia values make sense.

The system of equations was derived by analysing the reaction forces acting on each joint and the moments about each link. Newton's third law was also used to derive equations relating equal and opposite reaction forces. Using equations (1)-(13), a 13x13 matrix A can be formed and solved by rearranging the system of equations from $Ax = b$ into $x = bA^{-1}$. All reaction forces at each joint and the torque of the motor input link will be found by solving the following system of equations in MATLAB lines 40-52 of the file titled "dynamicAnalysis."

```

40 -    f12x = x(1,:);
41 -    f12y = x(2,:);
42 -    f23x = x(3,:);
43 -    f23y = x(4,:);
44 -    f32x = x(5,:);
45 -    f32y = x(6,:);
46 -    f34x = x(7,:);
47 -    f34y = x(8,:);
48 -    f43x = x(9,:);
49 -    f43y = x(10,:);
50 -    f14x = x(11,:);
51 -    f14y = x(12,:);
52 -    m12 = x(13,:);

```

Figure 28: Reaction forces and torque solved in Matlab

```

b = [m2*ag2x;
      m2*ag2y;
      i2*theta_2_a;
      m3*ag3x;
      m3*ag3y;
      i3*theta_3_a;
      m4*ag4x;
      m4*ag4y;
      i4*theta_4_a;
      0;
      0;
      0;
      0;];
x = A\b;

```

Figure 29: System of equations in Matlab

The torque of the input link vs θ_2 was graphed to determine any relationships. When analyzing the graph in figure #, the torque seems to vary in a parabolic pattern. This means that throughout the rotation of the link, the torque required to move the input link peaks at some point in the rotation where $\theta_2 \approx -0.9$ radians. The torque also becomes momentarily zero where the angle $\theta_2 \approx -1.6$ and $\theta_2 \approx -0.6$.

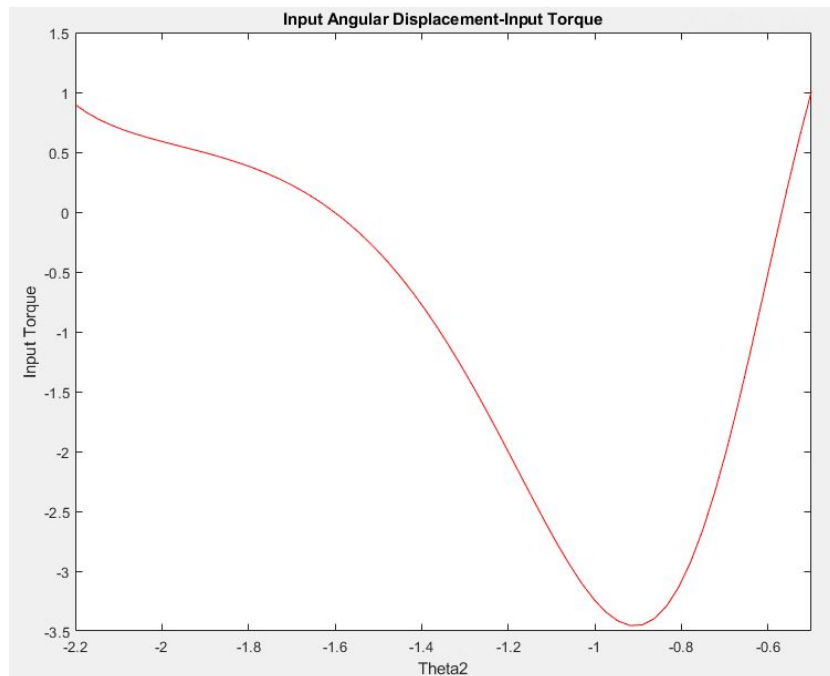
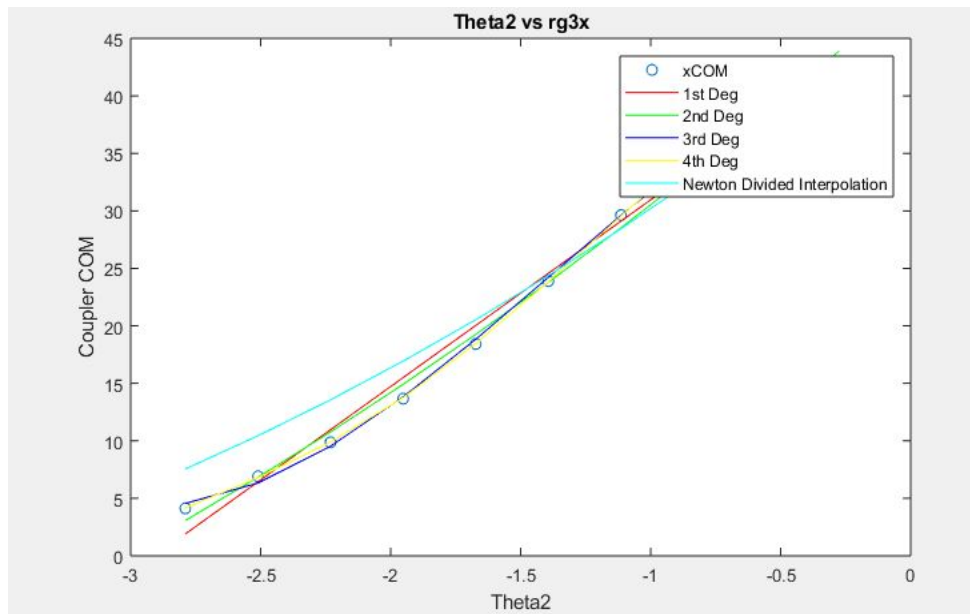


Figure 30: Graph of input torque vs θ_2

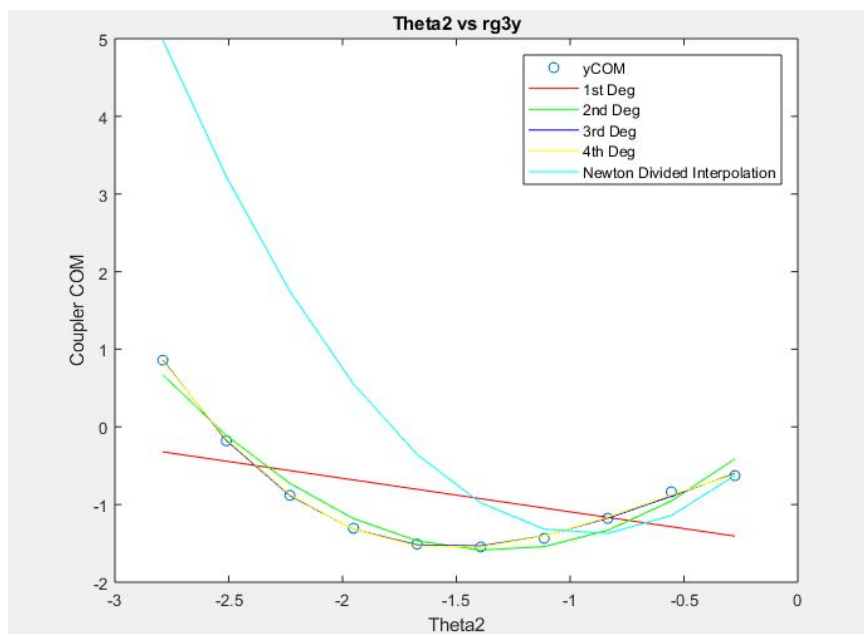
Coupler Curve Analysis

Curve fitting is used to get discrete data for obtaining intermediate estimates. Various methods of curve fitting were used to analyse coupler curve for all of the precision points. The first method used is least square regression to obtain first order, quadratic order , cubic order and higher order curve fits. Least square regression method is fitting straight line to pair observation, the objective of this is to minimize errors. The next method is interpolation method. Interpolation estimates the function value at intermediate point method the precision point/precise point. For this project, both these methods are used in calculating or analyzing the curve fit. The advantage of curve fitting is to model mathematical process gotten from the data; it makes it possible to estimate the parameter which gives an insight into the process.

The plot below shows the curve fit for first to fourth order interpolation and Newton divided difference interpolation coupler curve. This process was done by taking 10 points that go through the precision points and making a curve fitting model for it to give an estimate to the path. The 4 bar mechanism will go through the calculated curve and plot the graph of coupler vs theta 2 on MatLab. The plot clearly shows that our path is very similar to the curve fitting we are getting in the x-axis direction.

Figure 31: Graph of coupler vs θ_2 (x direction)

The plot below also shows the path we get after calculating the curve fit with least square regression and newton divided interpolation and this plot also shows that it is very similar to the path we are getting from the 4 bar mechanism in the y-axis direction. For this direction we did the same thing as for the x direction by taking 10 point from the precision point and making a curve fitting plot in Matlab to give the estimate of the process.

Figure 32: Graph of coupler vs θ_2 (y direction)

Conclusion

The 4-bar mechanism proposed for this project was successfully created and analysed in various approaches. When approaching the design of the mechanism, it was decided that the best algorithm to determine the design of the links was function generation. Since the precision points wanted were known, function generation was used to find the appropriate lengths of each link that resulted in the smoothest motion. Links 1 and 3 were calculated to be the same length, which seems incorrect, but calculations and animations show that these are the most appropriate lengths, with an Fval of 0.00013534.

The kinematic analysis allowed the observation of the linear velocities and accelerations of the center of masses of the input, coupler, and output links. As mentioned in the “Kinematic Analysis” section, the figures allowed the hypothesis that a mechanical singularity occurs when $\theta_2 \approx -2.75$ rad. This hypothesis was formed because the plots revealed that when $\theta_2 \approx -2.75$ rad the linear velocities and accelerations of the coupler and output links spiked to outlier values. This hypothesis continues to hold because the linear velocity and acceleration plots of the input link did not demonstrate the same spike. The input link’s did not and should not have a spike because the mechanical sensitivity in motion occurs only between the coupler and output link; the input link should continue to move controllably.

When the dynamics of the mechanism were inspected, a system of equations had to be solved to find the torque of the input link and reaction forces of each joint. A parabolic relationship between the torque and the reference angle, θ_2 , was found by graphing the two against each other.

The least squares regression method and the Newton method divided difference interpolation methods were used to curve fit a plot of the coupler’s centre of mass (COM) vs theta 2. When looking at the graphs in figures 31 & 32, it’s very clear that the more accurate method for the given data set is least squares regression. After the 4th iteration, the curve fit becomes very accurate to the plotted data points. Whereas the Newton divided difference method provides a poor representation of the plotted data points.

Overall, despite the said errors with velocity and acceleration analysis in the expanded numerical solution, the designed 4-bar mechanism gardening tool was successfully created and analysed using many methods. Each method produced accurate and similar results and the prototype showed smooth, curved motion, as expected. Future prototypes may follow these steps and get a reliable result.

References

Firmani, Flavio. Description of Final Project. MSE 211 Computational Methods for Engineers, 2019, *Description of Final Project 2019*.

Firmani, Flavio. Lab 1: Finding Roots. MSE 211 Computational Methods for Engineers, 2019, *Lab 1: Finding Roots*.

Firmani, Flavio. Lab 2: Optimization. MSE 211 Computational Methods for Engineers, 2019, *Lab 2: Optimization*.

Firmani, Flavio. Lab 2 - Project. MSE 211 Computational Methods for Engineers, 2019, *Lab 2 - Project*.

“Four-Bar Linkages.” *Four-Bar Linkages - OCW UPM - OpenCourseWare De La Universidad Politécnica De Madrid*, ocw.upm.es/ingenieria-mecanica/mechanical-devices-for-industry/contenidos/lectura-obligatoria/lesson-1/four-bar-linkages.

“Gardening Black Plastic Handle Dual Hoe Five Teeth Rake Shovel Outdoor Hoe Garden Tools - B0771D7QWP.” *Gardening Black Plastic Handle Dual Hoe Five Teeth Rake Shovel Outdoor Hoe Garden Tools: Kitchen & Home - B0771D7QWP*, www.coastandcountrylettings.co.uk/gardening-black-plastic-handle-dual-hoe-five-teeth-rake-shovel-outdoor-hoe-garden-tools-b0771d7qwp.html.